Antiviral Research 241 (2025) 106235

Contents lists available at ScienceDirect

Antiviral Research

journal homepage: www.elsevier.com/locate/antiviral

SARS-CoV-2 neutralization and protection of hamsters via nasal administration of a humanized neutralizing antibody

Mikhail Lebedin [a,b,*], Nikolai Petrovsky [c], Kairat Tabynov [d,e], Kaissar Tabynov [d,e,f,**], Yuri Lebedin [g,***]

[a] Max Delbrück Center for Molecular Medicine in the Helmholtz Association, 13125, Berlin, Germany
[b] Charité – Universitätsmedizin Berlin, Corporate Member of Freie Universität Berlin and Humboldt Universität zu Berlin, Charitéplatz 1, 10117, Berlin, Germany
[c] Vaxine Pty Ltd, 11 Walkley Avenue, Warradale, 5046, Australia
[d] International Center for Vaccinology, Kazakh National Agrarian Research University, 8 Abay Avenue, Almaty, 050010, Kazakhstan
[e] Preclinical Research Laboratory with Vivarium, M. Aikimbayev National Research Center for Especially Dangerous Infections, 14 Zhakhanger str., Almaty, 050054, Kazakhstan
[f] Republican Allergy Center, Research Institute of Cardiology and Internal Medicine, 120 Aiteke bi str., 050000, Almaty, Kazakhstan
[g] Xema Oy, Myllymäenkatu 21, 53550, Lappeenranta, Finland

ARTICLE INFO

Keywords:
SARS-CoV-2 antibodies
Intranasal administration
Prophylactic protective antibody
COVID-19
Antibody humanization

ABSTRACT

Monoclonal antibodies are widely used for the treatment of infectious human diseases, including COVID-19. Since the start of the pandemic, eight monoclonal antibodies against SARS-CoV-2 were granted emergency use authorization. The high mutation rate of the SARS-CoV-2 virus has led to the emergence of highly transmissible variants that can evade vaccine-induced immunity. In this study, we generated a panel of murine monoclonal antibodies (mAb) to identify a subset that broadly neutralized SARS-CoV-2 variants and explored whether mucosal administration of such antibodies could protect against infection. Intranasal delivery of XR10, the most promising murine mAb, protected hamsters against infection by Delta variant. We next humanized XR10 mAb using a combination of CDR-grafting and Vernier zones preservation approaches (CRVZ) to create a panel of humanized XR10 variants. We ranked the variants based on their spike binding ability and virus neutralization. Of these, XR10v48 demonstrated the best ability to neutralize SARS-CoV-2 variants and was protective in hamsters when given as a single 50 μg/kg intranasal dose at the time of viral challenge. XR10v48 featured 34 key amino acid residues retained from the murine progenitor. With SARS-CoV-2 escape mutants continuing to emerge this work highlights a potential workflow to generate humanized broadly cross-neutralizing mAb for potential use as a nasal spray for SARS-CoV-2 prophylaxis.

1. Introduction

Since the first outbreak in December 2019 (Huang et al., 2020), World Health Organization has reported 777.7 million cases of coronavirus disease 2019 (COVID-19) with the death toll reaching 7.0 million globally by April 2025 (https://data.who.int/dashboards/covid19). The causal agent, a beta coronavirus referred to as severe acute respiratory syndrome coronavirus 2 (SARS-CoV-2) (Cao et al., 2021), bears a spike protein crucial for binding the host receptor, angiotensin-converting enzyme 2 (ACE2) (Walls et al., 2020). Host receptor-spike interaction is mediated by a domain denoted as the receptor-binding domain (RBD) (Lan et al., 2020), which includes the receptor-binding motif (RBM), a major target of neutralizing antibodies (Ju et al., 2020). SARS-CoV-2 demonstrates a high mutation rate resulting in several variants of concern reported since the beginning of the pandemic, including Alpha (B.1.1.7), Beta (B.1.351), Gamma (P.1), Delta (B.1.617.2), Omicron (B.1.1.529), featuring higher severity of disease (Delta (Butt et al., 2022)) and transmissibility (Omicron (Fan et al., 2022)). Most mutations in the currently predominant Omicron variant are located in the spike RBD, which contributes to the virus immune evasion by reducing or completely abrogating the binding of neutralizing antibodies (Liu et al., 2022), thereby diminishing

* Corresponding author. Max Delbrück Center for Molecular Medicine in the Helmholtz Association, 13125, Berlin, Germany.
** Corresponding author. International Center for Vaccinology, Kazakh National Agrarian Research University, 8 Abay Avenue, Almaty, 050010, Kazakhstan.
*** Corresponding author. Xema Oy, Myllymäenkatu 21, 53550, Lappeenranta, Finland.
E-mail addresses: mikhail.lebedin@mdc-berlin.de (M. Lebedin), ktabynov@gmail.com (K. Tabynov), lebedin@xema.fi (Y. Lebedin).

https://doi.org/10.1016/j.antiviral.2025.106235
Received 27 April 2025; Received in revised form 9 June 2025; Accepted 5 July 2025
Available online 9 July 2025

vaccination efficiency (Hoffmann et al., 2022; Planas et al., 2022; Wang et al., 2021).

Since hybridoma technology was introduced in 1975 (Köhler and Milstein, 1975), monoclonal antibodies (mAbs) generated through mouse immunization have become a valuable tool in basic research and therapy. In 1986, the first murine mAb Muromonab-CD3 was approved by the United States Food and Drug Administration (FDA) to control kidney transplant rejection (Todd and Brogden, 1989). To date, 130 mAbs are approved for the treatment of various types of cancer, autoimmune disorders, and viral infections (Jacobson et al., 2009; Kempeni, 1999; Maloney et al., 1997; Pollack et al., 2002). So far, eight mAbs neutralizing SARS-CoV-2 were granted emergency use authorization (EUA): bamlanivimab, etesivimab, casirivimab, imdevimab, sotrovimab, cilgavimab, tixagevimab, bebtelovimab, with only the latter being effective in Omicron BA.1 cases (Westendorf et al., 2022).

Clinical application of mouse mAbs is rendered inefficient by human anti-mouse antibodies (HAMA), which can lead to accelerated mAb clearance in a high proportion of patients receiving such murine antibodies (Olsson et al., 1991; Shawler et al., 1985). Advances in genetic engineering and recombinant technology yielded several techniques that seek to overcome the HAMA response, including transgenic mice expressing human IgM, IgG, and IgK (Lonberg et al., 1994), human antibody phage display (Frenzel et al., 2016), and murine mAb humanization (Lu et al., 2023). Humanization aims to increase the similarity of the administered antibody to native human immunoglobulins, minimizing anti-drug reactivity and extending its half-life in the organism while retaining its antigen-binding properties (Lu et al., 2020). Several methods have been developed to achieve mAb humanization spanning from constant domain replacement (Investigators, 1994) to antibody resurfacing (Padlan, 1991) or specificity-determining residues grafting (Pascalis et al., 2002). Constant domain replacement was successfully used to reduce the immunogenicity of several FDA-approved chimeric antibodies including abciximab (Investigators, 1994), rituximab (Maloney et al., 1997), and cetuximab (Aboud-Pirak et al., 1988). Chimeric mAbs preserve murine content in the variable domain, presenting a potential target for HAMA response. The risk of the anti-drug response can be further decreased by complementarity-determining region grafting (CDR grafting) in which the murine CDRs are transplanted onto the human frameworks (FRs) (Ferrara et al., 2004). In most cases, direct grafting of the CDR loops onto human FRs leads to substantial loss of target affinity (Pavlinkova et al., 2001). Several buried residues comprising the β-sheet framework regions, referred to as Vernier zones residues (VZRs), were reported to influence the conformation of the CDR loops, therefore affecting the antigen binding (Foote and Winter 1992; Makabe et al., 2008). Therefore, CDR grafting should be accompanied by transferring the corresponding VZRs while controlling the affinity of the humanized antibody.

Here we report the generation of a large panel of murine mAbs, a subset of which potently neutralized a range of SARS-CoV-2 variants. The lead candidate, XR10, was protective when delivered nasally in a hamster challenge model and was then humanized by the CRVZ approach. We selected a humanized variant with the highest neutralizing activity and demonstrated its intranasal effectiveness against the SARS-CoV-2 Delta strain in a hamster challenge model.

2. Materials and methods

2.1. Mouse immunization

Four-to-six-week-old female BALB/c mice were immunized 4 times every three weeks with 50 μg of the Wuhan Spike or RBD protein via intraperitoneal injection with complete Freund's adjuvant. After 4 doses of the same injection, the response potency was estimated using antigen ELISA. A booster dose was injected for high responders 20 days after the fourth immunization. 4 days after the boost, mice were sacrificed and spleens were harvested.

2.2. Hybridoma generation

Splenocytes of the mice were harvested and fused with mouse myeloma SP2.0 cells. Fused cells were cultured in DMEM supplemented with 10 % FBS, HAT medium, hybridoma growth factors in 96-well culture plates. 2 weeks after fusion, the supernatants were analyzed for antibody titer with ELISA. Selected clones were subcloned via limiting dilution.

2.3. ELISA

In-house-produced recombinant RBD was immobilized on a high-binding 96 well ELISA plate (Corning, #CLS3690) at 4 μg/ml in PBS (Sigma-Aldrich, MO, USA) overnight at +4 °C. Plates were blocked for 1 h with 1 % BSA (Thermo Fisher, Gibco, MA, USA) in PBS at room temperature. Antibodies were diluted in PBS 1 % BSA to indicated serial dilutions, added to coated plates and incubated for 1 h at room temperature. Plates were developed with an anti-human IgG-alkaline phosphatase (AP)-coupled antibody (SouthernBiotech #2040-04) diluted 1:500 in PBS 1 % BSA. Bicarbonate buffer with 4-Nitrophenyl phosphate disodium salt hexahydrate substrate (Sigma-Aldrich, #S0942-50TAB) was added and absorbance was measured at 405 nm in a Cytation 5 device (BioTek). Between all indicated incubation steps, plates were washed 3 times with PBS 0.05 % Tween-20. 50 % of maximum IgG binding to RBD or nucleocapsid (ED50) was determined for each sample by sigmoid curve fitting with non-linear regression performed in R (stats package) (RCoreTeam, 2019). For curve fitting, upper and lower plateaus of the reference antibody (murine antibodies) were applied to all samples. The positive control was used to normalize independent measurements.

2.4. Competition ELISA

Upon 1 h blocking with PBS/1 % BSA, serially diluted antibodies in PBS/1 % BSA were added to SARS-CoV-2 RBD-coated (10 μg/ml) 96 well plates. After 1 h of incubation at room temperature, self-produced biotinylated human ACE2-hFcg1, EY6A, P2B-2F6, P2C-1F11, REGN10933, REGN10987, CC12.1, C144, S2H13, S309, 4A8 were added to a 50 % final effective concentration (EC_{50}) in PBS/1 % BSA for competition with monoclonal antibodies. After another hour at room temperature, plates were incubated with an AP-coupled streptavidin (SouthernBiotech, #SBA-7105-04) at a 1:500 dilution in PBS/1 % BSA to detect biotinylated ACE2-hFcg1 that was not prevented by serum antibodies from binding to RBD. The 50 % blocking dose (BD_{50}) was determined by sigmoid curve fitting with non-linear regression performed in R (stats package). Upper and lower plateaus of the (non-)biotinylated ACE2-hFcg1 control served as a reference.

2.5. Monoclonal antibody sequencing

Sequencing of XR10, XR14, and XR51 antibodies was performed by Absolute Antibody Ltd (UK) by whole transcriptome shotgun sequencing (RNA-Seq).

2.6. Recombinant proteins cloning

SARS-CoV-2 RBD WT was cloned containing the signal peptide spanning amino acids M1-Q14 and R319-F541 of the pCAGGS-SARS-CoV-2 RBD Wuhan plasmid (kindly provided by F. Krammer; GenBank: MN908947.3, (Amanat et al., 2020)), followed by a C-terminal Twin-Strep-tag sequence (WSHPQFEKGGGSGGGSGGSAWSHPQFEK) and a hexahistidine tag. SARS-CoV-2 spike encoding plasmid comprised the amino acids M1-Q1208 of the Wuhan SARS-CoV-2 variant (GenBank: MN908947.3) with Furin cleavage site mutations (682–685 RRAR -> QQAQ) as well as 6 Proline mutations (HexaPro) to generate a protease-resistant, stable and highly immunogenic SARS-CoV-2 spike

protein locked in the pre-fusion conformation followed by a Twin-Strep-tag and a hexahistidine tag. For expression of the membrane-bound version, a SARS-CoV-2 spike full-length vector with a C-terminal 19 amino acid deletion comprising amino acids M1-C1254 of the Wuhan SARS-CoV-2 variant (GenBank: MN908947.3) was used. Mutations of RBD and full spike were introduced by PCR mutagenesis. The N-terminal domain (amino acids M1-S305) of the SARS-CoV-2 spike was cloned to a C-terminal Twin-Strep-tag and a hexahistidine tag. Plasmids containing human full-length ACE2 (Clone: OHu20260C; M1-F805) and rabbit full-length ACE2 (Clone: OOb21562C; M1-F805) C-terminally linked to enhanced green fluorescent protein (eGFP) were purchased from GenScript (GenScript Biotech Netherlands B.V.). Heavy and light chain sequences of humanized and control mAbs were synthesized by oligonucleotide assembly and cloned using Gibson assembly (NEBuilder HiFi DNA assembly kit, NEB, #E5520S) into IgG1 heavy and kappa or lambda light chain expression vectors from Oxgene (Sigma-Aldrich; #PP2409-1 KT): class 1–4 anti-SARS-CoV-2 RBD: EY6A, P2B-2F6 and P2C-1F11, REGN10933 and REGN10987, CC12.1, C144, S2H13, S309, anti-SARS-CoV-2 NTD: 4A8. Framework reshuffling for humanized mAbs was performed using framework and CDRs amplification and subsequent Gibson assembly. Human ACE2-hFcg1 was produced by fusing recombinant human ACE2 Q18-V739 fragment to human IgG1-Fc (E99-K330 portion, where the first amino acid is G encoded by J-CH1 fusion).

2.7. HEK cell recombinant protein production

Cloning constructs were used to transfect FreeStyle 293-F cells that were grown in suspension using FreeStyle 293 expression medium (Life Technologies, #A1435101) at 37 °C in a humidified 8 % CO2 incubator rotating at 125 rpm. Cells were grown to a density of 2.5 million cells per ml, transfected using polyethyleneimine (PEI, Polysciences Europe GmbH; #23966-1; 4 μg/ml in cell suspension) and DNA (1200 ng/ml in cell suspension), and cultivated for 3 days. The supernatants were harvested and proteins purified by His SpinTrap columns (for His-tagged antigens) or Protein G columns (for the antibodies) according to the manufacturer's instructions (Cytiva, His: #28-9321-71, Ab: #28-4083-47). The eluted protein was transferred to phosphate-buffered saline (PBS) via buffer exchange using Amicon Ultra-4 ultrafiltration column with 50 kDa or 10 kDa cutoff (Millipore, #UFC805008, #UFC801096). Protein concentration was determined by His-tag specific ELISA using a mouse anti-His-tag antibody (Abcam, #ab18184) and a goat anti-mouse IgG Fc antibody conjugated to alkaline phosphatase (SouthernBiotech, #SBA-1033-04) as a detection reagent. Antibody concentration was determined by absorbance measurement at 280 nm. Protein production was confirmed by SDS-PAGE and Western blot using a mouse anti-His antibody (Abcam, #ab18184) and an IRDye 800CW donkey anti-mouse antibody (Li-Cor Biosciences, #925–32212).

2.8. Insect cell recombinant spike protein production

The antigen in SpikoGen® vaccine corresponds to aa 14–1213 of the spike protein sequence of the ancestral Wuhan-Hu-1 strain (accession number: NC 045512) with various modifications, as previously described [18]. In this study, Wuhan, Beta and Gamma, Delta and Omicron spike proteins were manufactured using the same process as the human approved SpikoGen® vaccine. Spike antigens and Advax-CpG55.2 adjuvant were provided by Vaxine Pty Ltd, Adelaide, Australia.

2.9. Administration of monoclonal antibody to hamsters and their SARS-CoV-2 virus challenge

Each of the monoclonal antibody preparations XR10 (1.24 mg/mL) and XR10RH (4.73 mg/mL) were diluted with DMEM at a final concentration of 5.5 μg/100 μL or 50 μg/kg, and antibodies or PBS intranasally administered to 6-8-week-old male Syrian hamsters (50 μL in each hamster nostril, n = 4/group) under intraperitoneal ketamine (100 mg/kg) and xylazine (10 mg/kg) anesthesia (Table 1). Syrian hamsters were obtained from the laboratory animal nursery of the M. Aikimbayev National Scientific Center for Especially Dangerous Infections (NSCEDI, Kazakhstan) and during the experiment housed in an individually ventilated system with a 30-cage ventilated rack in the ABSL-3 laboratory of NSCEDI. Two hours later, the hamsters of groups 1–3 under anesthesia were intranasally infected with the strain hCoV-19/Kazakhstan/KazNARU-NSCEDI-5526/2021 of Delta variant SARS-CoV-2 virus (full protein sequence was published in GISAID database under number EPI_ISL_4198501) at a dose of $10^{6.0}$ $TCID_{50}$/100 μL (50 μL per nostril) as previously described (Solomadin et al., 2023). Animals of the negative control group, which were kept in a separate room of the ABSL-3 laboratory from the experimental groups, were subjected to a similar anesthesia procedure. Infected animals were clinically monitored from day 0 to day 3, and their weight was measured daily. On day 3 after the challenge, animals from each group were sacrificed, and samples from nasal turbinates and lungs were collected. The lungs of the animals were evaluated for the level of lesions by the area of hemorrhage in the JMicroVision program (v 1.3.4). The percentage ratio of the area of the affected areas to the total area of the lung surface was studied. Two lobes of the left lung were homogenized in 1 ml of DMEM using a TissueLyser II (QIAGEN) device at 300 vibrations per minute for 60 s. The supernatant obtained after centrifugation (5000 g for 15 min at 4 °C) was stored at −70 °C for the determination of the virus titer. Three right lung lobes of each animal were fixed in 10 % formalin for histopathological examination to confirm detected lung lesions.

2.10. Determination of the infectious virus titer

Virus titers in homogenates of respiratory tract tissues were determined using the 50 % tissue culture infectious dose ($TCID_{50}$) analysis. The tissue homogenates were diluted ten-fold in a medium (DMEM-2 % FCS-1 % antibiotic-antimycotic) and transferred in quadruplicate into 96-well plates containing Vero-E6 confluent cells. The plates were then incubated at 37 °C and 5 % CO_2 for 5 days to ensure complete cytopathic effect (CPE) development, especially for samples with low viral titers. This extended incubation period is a recognized modification for slow-replicating strains and ensures accurate endpoint detection. The titration results were visually calculated by studying the cellular monolayer under a microscope for specific cytopathic effects such as cell rounding and cell separation from the monolayer. The viral titer was determined using the Reed and Muench method and expressed as $\log_{10}$ $TCID_{50}$/mL.

2.11. Histological analysis of hamster lungs

The lungs of hamsters were fixed in 10 % neutral buffered formaldehyde after excision, washed with water, and treated with four portions of 100 % isopropyl alcohol and two portions of xylene. The material was then soaked in four portions of paraffin, and blocks were created. Histological blocks were sectioned to a thickness of 5 μm using a microprocessor microtome MZP-01 (CB Technom, Russia). The sections were dewaxed in two portions of xylene and three portions of ethyl alcohol with reduced concentrations (96 %, 80 %, 70 %), then stained with hematoxylin (#05-002, BioVitrum, Russia) and eosin (#C0362, DiaPath, Italy). Subsequently, the sections were clarified in increasing concentrations of ethyl alcohol (70 %, 80 %, 96 %) and two portions of xylene. The sections were covered with glass coverslips using the synthetic medium Bio Mount (#2813, Bio Optica, Italy). The slides were examined using the Mshot microscope (China), model MF52-N. Photos were taken with a magnification of ×40 using Mshot MS23 camera tips (China) and the MShot Image Analysis System program (China). Microscopic examination of the lungs followed classical canons adopted for parenchymal organs, and the description of pathological conditions induced by SARS-CoV and SARS-CoV-2 was used for narration. Each slide was quantitatively assessed based on the severity of histological

Table 1
Study design.

Group number	Preparation	Preparation dosage	Administration route	Virus dose ($TCID_{50}$)	No. of animals
XR10 mouse mAb					
1	XR10 (mouse)	mAb 50 μg/kg	Intranasal	10^6	4
2	Positive control (virus)	100 μl PBS	Intranasal	10^6	4
3	Negative control (DMEM)	100 μl PBS	Intranasal	–	4
XR10RH humanized mAb					
4	XR10RH (humanized)	mAb 50 μg/kg	Intranasal	10^6	4
5	Positive control (virus)	100 μl PBS	Intranasal	10^6	4
6	Negative control (DMEM)	100 μl PBS	Intranasal	–	4

changes, including interstitial pneumonia, alveolitis, bronchiolitis, alveolar destruction, interstitial infiltration, pulmonary hemorrhage, and peribronchiolar inflammation. Histopathological evaluation was performed under blinded conditions using a semi-quantitative scoring system to assess the severity of inflammation and tissue damage. Scores were defined as follows: Score 0 – no pathological changes (0 % of tissue affected); Score 1 (mild) – inflammation involving <25 % of the lung section, characterized by sparse perivascular or peribronchiolar infiltration with ≤2 cell layers of inflammatory cells; Score 2 (moderate) – involvement of 26–50 % of tissue, with multifocal infiltration of 3–4 cell layers, mild alveolar wall thickening, and occasional epithelial cell desquamation; Score 3 (marked) – inflammation affecting 51–75 % of lung area, with 5–6 layers of mononuclear infiltration, moderate alveolar collapse, and bronchiolar epithelial damage; Score 4 (severe) – diffuse inflammation involving >75 % of lung tissue, dense cellular infiltration (>6 layers), extensive alveolar consolidation, hemorrhage, and epithelial necrosis. These criteria were designed to reduce subjectivity and improve reproducibility across independent evaluators.

2.12. Biosafety and bioethics

All operations involving SARS-CoV-2 and viral experiments on animals were conducted in the BSL-3 and ABSL-3 laboratories of NSCEDI, where the international standard ISO 35001:2019 “Biological Risk Management for Laboratories and Other Related Organizations” was followed. Laboratory animals were housed in individually ventilated cages (Techniplast, Italy, and Allentown, USA) under a 12/12 day and night cycle. This study was conducted in compliance with national and international laws and guidelines for the handling of laboratory animals. The protocol was approved by the Institutional Animal Care and Use Committee of the National Scientific Center of Especially Dangerous Infections, Protocol No. 4, dated September 22, 2020.

2.13. Statistical analysis

The statistical data analysis was performed using the GraphPad Prism program, version 9.0.0 (San Diego, California, USA) and R, version 4.3.1 (RCoreTeam, 2019). Differences in weight loss, viral load, and pathological changes in the lungs between the groups of animals were assessed using the Tukey multiple comparison test. A Shapiro-Wilk test was used for normality testing of continuous variables. An independent *t*-test was used when continuous data met the criteria of the normality test. Otherwise, the Mann-Whitney *U* test was used. Spearman correlations were performed with a 95 % confidence interval. The limit of detection for viral titer was 0.7 $\log_{10}$ $TCID_{50}$/0.2 mL. A p-value of less than 0.05 was considered statistically significant for all comparisons. Figures were generated using R ggplot2 package, Inkscape software, and BioRender.

2.14. Protein structure analysis

Antibody structures were predicted using templated AlphaFold-2 software (Jumper et al., 2021). Antibody-antigen interaction was analyzed using the HDOCK server. Protein structures and interactions were analyzed and depicted with UCSF ChimeraX 1.7.3. The following PDB codes were used: 6M0J for SARS-CoV-2 RBD and ACE2 (Lan et al., 2020), 6ZER for EY6A (Zhou et al., 2020), 6XC3 for CC12.1 (Yuan et al., 2020), 8DCC for P2B-2F6 (Dickey et al., 2022), 8GX9 for P2C-1F11 (Wang et al., 2022), 6XDG for REGN10933 and REGN10987 (Hansen et al., 2020), 7K90 for C144 (Barnes et al., 2020), 7JV2 for S2H13 (Piccoli et al., 2020), 7XSW for S309 (Jia et al., 2022), 8DM4 for 4A8 (Saville et al., 2023).

3. Results

3.1. Generation of murine SARS-CoV-2 neutralizing antibodies

To generate the mAbs, we immunized BALB/c mice with Wuhan SARS-CoV-2 Spike protein and used hybridoma technology to create the clones (Fig. 1A). Purified mAbs were tested for binding to Spike and RBD proteins from various virus strains and virus neutralization (Fig. 1B).

XR10, XR14, and XR51 mAbs featured high binding to various Spike proteins, >90 % inhibition of ACE2-RBD binding, and highest neutralizing activity (IC_{50} = 17.7, 28.8, 12.2 ng/ml for XR10, XR14, and XR51, accordingly) toward the Wuhan variant and were selected for humanization. While XR14 was not able to neutralize Delta or Omicron BA.1 variants, XR10 showed moderate neutralization capacity against Omicron BA.1 (410 ng/ml) and XR51 neutralized the Delta variant with IC_{50} 65.5 ng/ml (Fig. 1B–Table S1).

3.2. mAbs epitope characterization

To map the epitope targeted by the selected mAbs *in vitro*, we performed a binding competition assay with ACE2 and a panel of previously characterized antibodies (Chi et al., 2020; Ge et al., 2021; Hansen et al., 2020; Piccoli et al., 2020; Pinto et al., 2020; Robbiani et al., 2020; Rogers et al., 2020; Wu et al., 2010; Zhou et al., 2020) (Fig. 1C–Table S1). We used the antibodies representative of different classes: class 1 defined by targeting the RBM in “up” conformation; class 2 that bind the RBM in both “up” and “down” conformations; class 3 that bind outside of ACE2-interacting interface but are able to hinder the host receptor interaction; and class 4 that do not perturb the ACE2-RBD binding (Chen et al., 2023). All three mAbs competed moderately with ACE2-hFcg1 binding (44.0 %, 42.4 %, 47.7 % inhibition for XR10, XR14, and XR51) and demonstrate >80 % binding inhibition by such class 1 antibodies as REGN10933 (90.4–95.9 %), P2C-1F11 (81.5–88.4 %), C144 (80.8–84.5 %), and CC12.1 (80.8–86.7 %). All selected antibodies competed moderately with class 2 antibodies, as P2B-2F6 (56.6–62.9 %) and S2H13 (69.0–73.6 %) and competed weakly with S309, which is classified as an epitope 3 antibody (9.9–28.5 %). Surprisingly, XR14 showed 79.8 % binding inhibition for the class 4 antibody EY6A. Cross-inhibition assay shows that XR10 epitope overlapped with both XR14 and XR51 interaction zones (93.1 % and 91.8 % inhibition, correspondingly), while we detected a weak inhibition for XR51-XR14 binding (38.2 %). These data suggest that XR10 and XR51 bind an RBM epitope and are closely related to class 1/2 Abs, while XR14 might demonstrate a unique multimodal binding overlapping with class 1/2 and class 4 Abs.

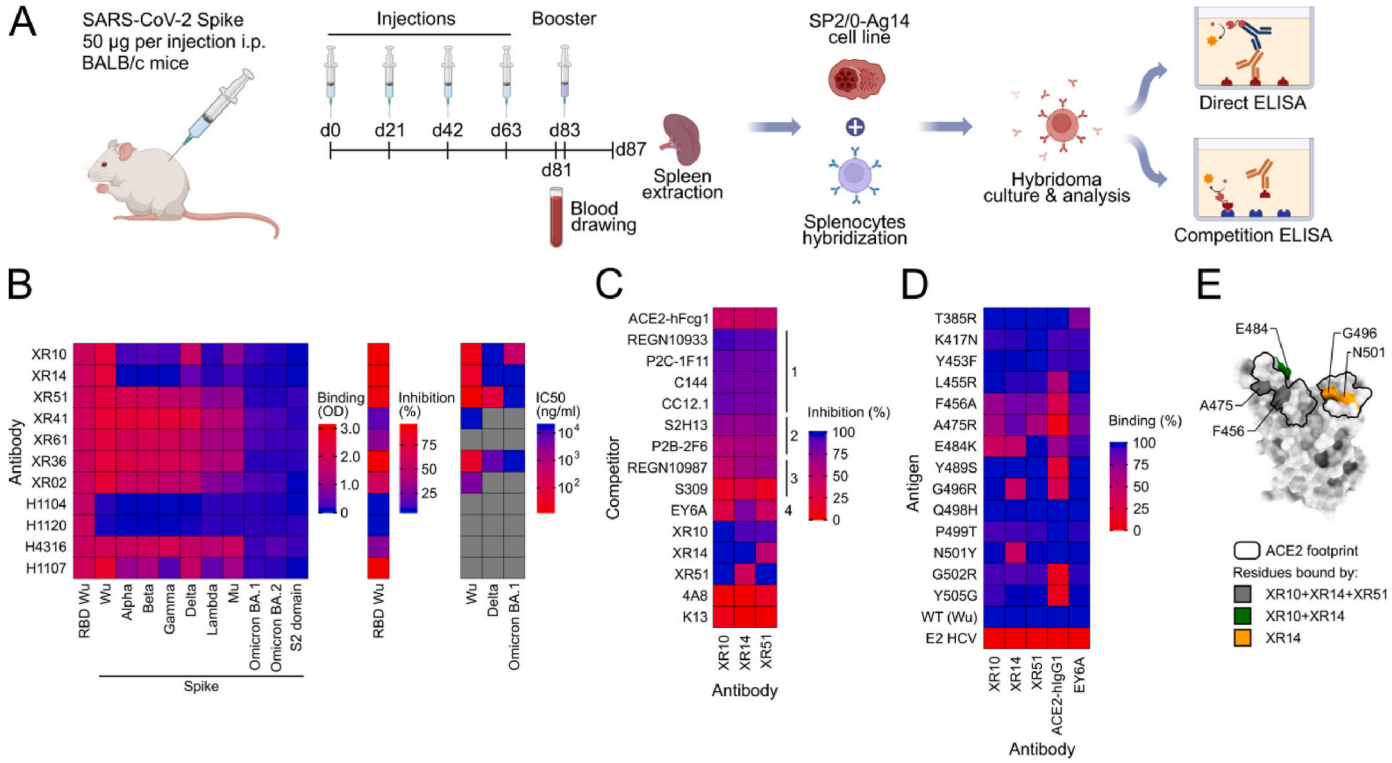

Fig. 1. A set of mAbs against SARS-CoV-2 Spike efficiently bind and neutralize various viral strains. (A) Scheme depicting mice immunization, hybridoma generation, and mAb analysis. **(B)** mAbs were screened for binding to a diverse set of SARS-CoV-2 Spike proteins (on the left), for inhibition of ACE2-Wuhan RBD binding (middle), and neutralization of the live viruses (on the right). H1104, H1120, H4316, H1107 – commercial antibody controls. **(C)** Wuhan RBD binding competition with various antibodies interacting with distinct epitopes on the RBD surface. K13 - anti-human CD81 antibody used as a negative control. **(D)** mAb binding to a set of Wuhan RBD mutants. E2 - hepatitis C virus surface protein subunit used as a negative control. **(E)** Residues affecting the XR mAbs binding and the ACE2 footprint were mapped on the Wuhan RBD surface.

To define the epitopes on the amino acid residue level, we performed binding assay with various Wuhan RBD mutants. Mutations F456A, A475R, E484K, located within class 1/2 epitopes, substantially decreased the binding of XR10 and XR14 mAbs, while XR51 bound to E484K mutant with nominal affinity (Fig. 1D–Table S1). While not affecting XR10 and XR51, mutations G496S and N501Y, located in the right shoulder of RBD (Fig. 1E) (Dejnirattisai et al., 2021), reduced the XR14 binding to 43.1 % and 42.2 %, accordingly. These data are in agreement with competition analysis and indicate that all three antibodies belong to class 1 and class 2 antibodies. Furthermore, the XR10 epitope overlapped with both XR14 and XR51 interaction zones, while XR14 and XR51 featured distinct modes of binding.

3.3. XR10, XR14, and XR51 humanization

To humanize the selected mouse antibodies, we identified the human germline (HGL) heavy and light chain variable domain sequences of the highest homology by aligning the murine AA V(D)J sequences to the library of human segments using IgBLAST (Fig. S1). We assumed no junctional diversity (no P/N-nucleotides addition) when reconstructing HGL sequences. We introduced the humanization index (DtH, distance to human, indicating the total number of AA exchanges needed to be introduced in heavy and light variable domains to arrive to the HGL sequence) to reflect the depth of humanization. Mouse XR10, XR14, and XR51 display DtH of 57, 69, and 50 AAs exchanges, correspondingly (Fig. S1). Taken that the total length of heavy and light chain variable domains is 231, 226, and 235 AAs for XR10, XR14, and XR51, it translates to 75.3 %, 69.5 %, and 78.7 % homology to HGL, respectively. CDRs predicted by IgBLAST software were grafted into fully human frameworks and constant regions were replaced with human IgG1 or IgK (CG version, Table S2). Additionally, we attempted to replace the amino acid residues located on the flanks of CDR loops to create deeply humanized mAb variants (DH, Table S2). CDR grafting decreased DtH from 57, 69, 50 to 24, 19, 12 (89.6 %, 91.6 %, 94.9 % homology to HGL) for XR10, XR14, and XR51, correspondingly, while deep humanization minimized the DtH to 12, 11, 3 (94.8 %, 95.1 %, 98.7 % homology to HGL). Binding analysis revealed a drastic drop in affinity for humanized antibodies with only CG-XR10 binding to Wuhan RBD with <1.0 ng/µl EC_{50} (Fig. 2A, Table S1). These results indicate a significant contribution of Vernier zones residues (VZRs) to antigen recognition. To locate the critical VZRs we assessed the contribution of the heavy and the light chains by generating all combinations of the murine, CG, and DH variants (Fig. 2B). For XR10 and XR14 the binding is governed by both chains, while for XR51, the nominal binding is retained if the original murine heavy chain is coupled with any light chain variant, pointing to virtually exclusive heavy chain-mediated binding (Fig. 2B–Table S1). To further narrow down the location of the critical VZRs, we performed framework reshuffling for both chains of XR10 and XR14 (Fig. 2C and D, Table S1) and for heavy chain of XR51 (Fig. 2E–Table S1). Surprisingly, XR51 framework reshuffling revealed all-or-nothing effect of heavy chain FR2 and FR3 mutagenesis, i.e. the mAb binds Wuhan RBD with original affinity only if both HC FR2 and FR3 are not humanized. This allowed us to isolate the critical VZRs for XR51 heavy chain. While A50 is immediately adjacent to CDR2, K67, A68, L70, A72, and S76 are located in the middle of FR3 with CDR2-proximal FR3 residues (S59, N61, R63, K65) being insensitive to humanization. These data suggest that Vernier zone residues shall be identified experimentally as they might be located in buried sites outside of interaction zone. We summarized an experiment-driven humanization pipeline by CDR-grafting and Vernier zone preservation approach (CRVZ) in Fig. S2. Of note, Humanization yielded XR10v43 and XR51v127 variants with high level of humanization and nominal or higher-than-nominal binding strength

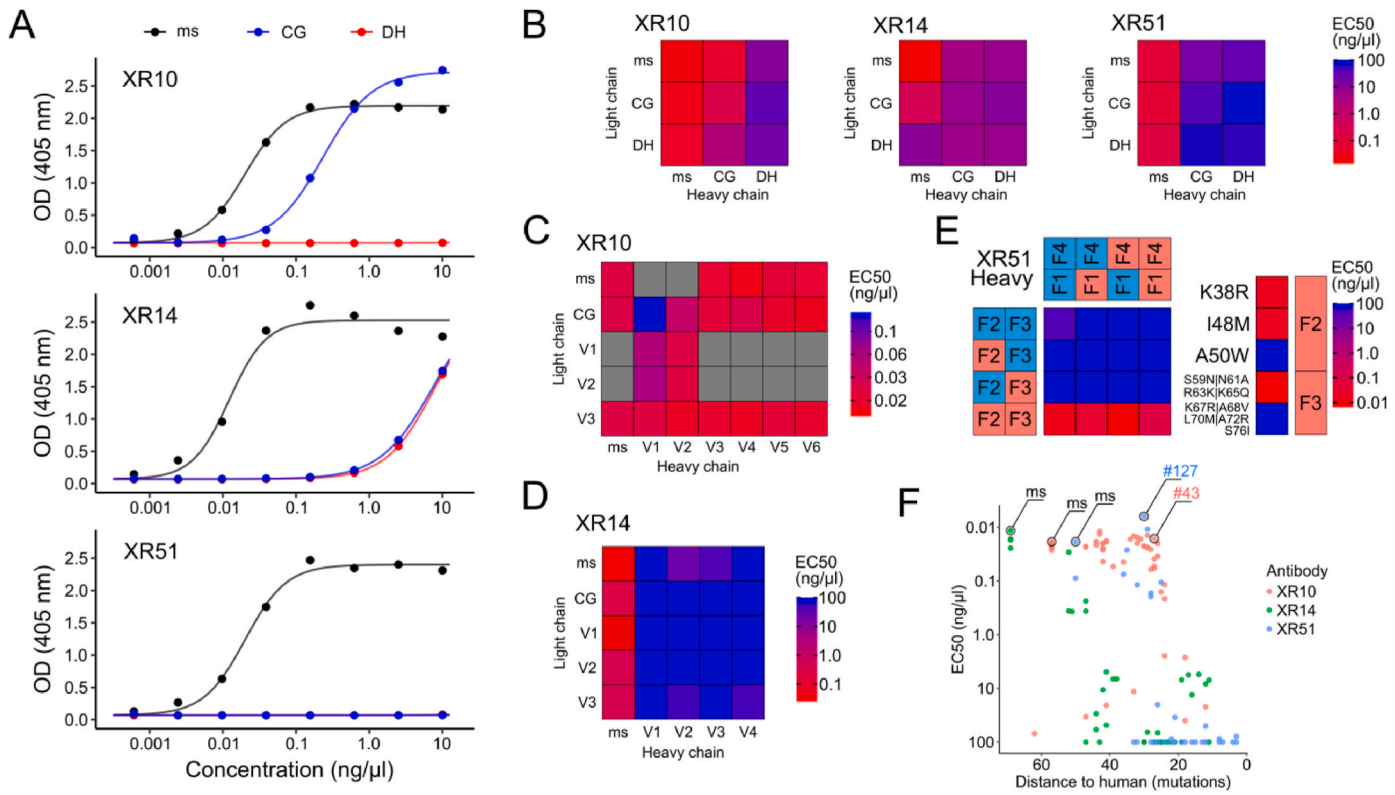

Fig. 2. XR antibody humanization yielded highly humanized XR10 and XR51 variants with nominal binding affinity. (A) Mouse, CG, and DH variants binding. **(B)** Binding of XR antibodies generated by reshuffling of ms, CG, and DH heavy and light chains. **(C)** Binding of XR antibodies generated by framework reshuffling for XR10 **(C)** and XR14 **(D)** heavy and light chains, and for heavy chain of XR51 **(E)**. **(F)** Binding of XR variants plotted against the level of humanization. All binding assays performed with SARS-CoV-2 Wuhan RBD. OD - optical density, EC50 - effective dose 50 %. CG - CDR-grafted version, DH - deeply humanized version.

(XR10v43: DtH = 27, 88.3 % homology to HGL, EC_{50} = 0.016 ng/µl; XR51v127: DtH = 30, 87.2 % homology to HGL, EC_{50} = 0.006 ng/µl, Fig. 2F–Table S1). We compared our humanization pipeline to previously published machine-learning approach called Hu-mAb (Marks et al., 2021). Predicted humanization mutations mostly overlap with the set introduced in this study, although Hu-mAb uses different germline segments for XR10 and XR51 kappa chains (Fig. S1). Humanness score estimated by Hu-mAb strongly correlated to DtH (r = −0.91) while offering more discrete values (Fig. S3A). Binding strength demonstrated similar dependence from humanness score in comparison to DtH (Fig. S3B). Therefore, both approaches can be used to assess the extent of humanization and design a humanized mAb sequence.

3.4. *Different XR10 Vernier Zone residues contribute to Wuhan and Omicron BA.1 binding*

In order to study how the humanization influences the binding of XR10 to different SARS-CoV-2 strains, we generated 110 antibody variants by reshuffling frameworks and chains of XR10 (Table S2, Fig. S1) and tested their binding against Wuhan and Omicron BA.1 RBD (Fig. 3A and B, Table S1). Only a minor fraction of the variants bound Omicron BA.1 RBD with affinity comparable to their anti-Wuhan interaction (Fig. 3C, Fig. S4A). DtH analysis revealed that Omicron BA.1 binding is extremely sensitive to humanization, with no variants of DtH≤35 binding with nominal affinity (Fig. 3D). We hypothesized that Omicron BA.1 binding is influenced by a different set of AA exchanges introduced with the humanization, hence we used decision tree regression to determine the relative contribution of the mutated residues (Fig. 3E). While humanizing H69, H102, and K37 residues (H – heavy, K – kappa) affect both Wuhan and Omicron BA.1 binding, H31 influences Wuhan binding exclusively and K58 and K84 contribute to Omicron BA.1 binding (Fig. 3F). Mapping the residues on AlphaFold-generated msXR10 model demonstrated that K58 and K84 residues are distant from the paratope (Fig. 3G) (Jumper et al., 2021). These results suggest a distinct mode of XR10-Omicron BA.1 interaction, where K58 and K84 AAs are critical for Omicron BA.1 binding proficient paratope folding.

3.5. *XR10v48 anti-SARS-CoV-2 mAb intranasal prophylactic protection in hamsters*

In order to test how the humanization affected the neutralization potency of XR10 *in vivo*, we selected the most potent XR10 variants (EC_{50} < 1 ng/µl, XR10v51 as a low-affinity control) with DtH≤41 for further experiments (Fig. S4A). We tested the selected variants in live virus neutralization for Wuhan, Delta, and Omicron BA.1 strains (Fig. S4B). XR10v48 demonstrated the best combination of humanization extent (DtH = 34, 85.3 % homology to HGL), viral neutralization (IC_{50} of 3.0, 2.4, and 12.3 ng/µl for Wuhan, Delta, and Omicron BA.1, correspondingly) and higher affinity in comparison to mouse mAb (0.917 nM versus 1.167 nM for msXR10, Fig. S5, Table S1). To evaluate XR10v48 performance in hamster protection, we administered 50 µg/kg of either humanized or mouse mAb intranasally simultaneously with SARS-CoV-2 Delta (B.1.617.2) variant infection (4 animals per group, 10^6 TCID50 per animal). Hamsters that received either mouse or humanized mAb, demonstrated a significant reduction of weight loss (Fig. 4A and B). Although we did not detect significant decrease of SARS-CoV-2 load in nasal turbinates, lung viral load was significantly reduced both in mouse XR10 (Fig. 4C) and XR10v48 administration (Fig. 4D). We assessed the pulmonary damage by hemorrhagic foci counting (Fig. 4E and F) and lung lesion score (see Methods, Fig. 4G and H). For both the mouse XR10 and humanized XR10v48 treatment groups, lesions were less pronounced than in challenge-only controls (Fig. 4E–H). These data

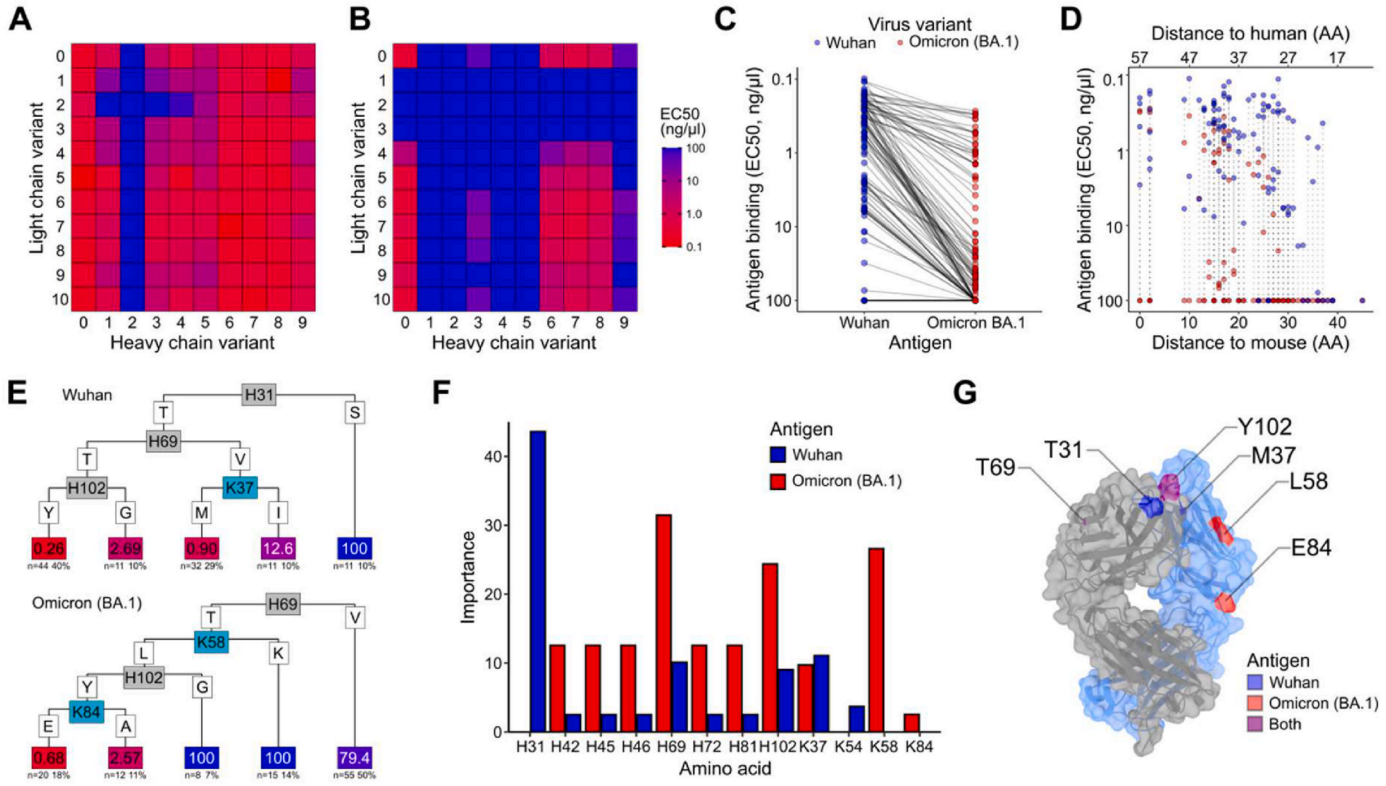

Fig. 3. Different Vernier zone residues are contributing to XR10 binding to Wuhan and Omicron BA.1 SARS-CoV-2 RBD. All combinations of framework reshuffled XR10 heavy and light chains were expressed and profiled by binding to Wuhan **(A)** and Omicron BA.1 RBD **(B)**. **(C)** XR10 variants binding to Wuhan Omicron BA.1 RBD. **(D)** Binding to Wuhan and Omicron BA.1 RBD versus distance to human. **(E)** Decision tree regression analysis performed for Wuhan and Omicron BA.1 RBD binding **(F)** Contribution of individual Vernier Zones amino acid residues to RBD interaction. **(G)** Crucial amino acid residues mapped on the predicted mouse XR10 model.

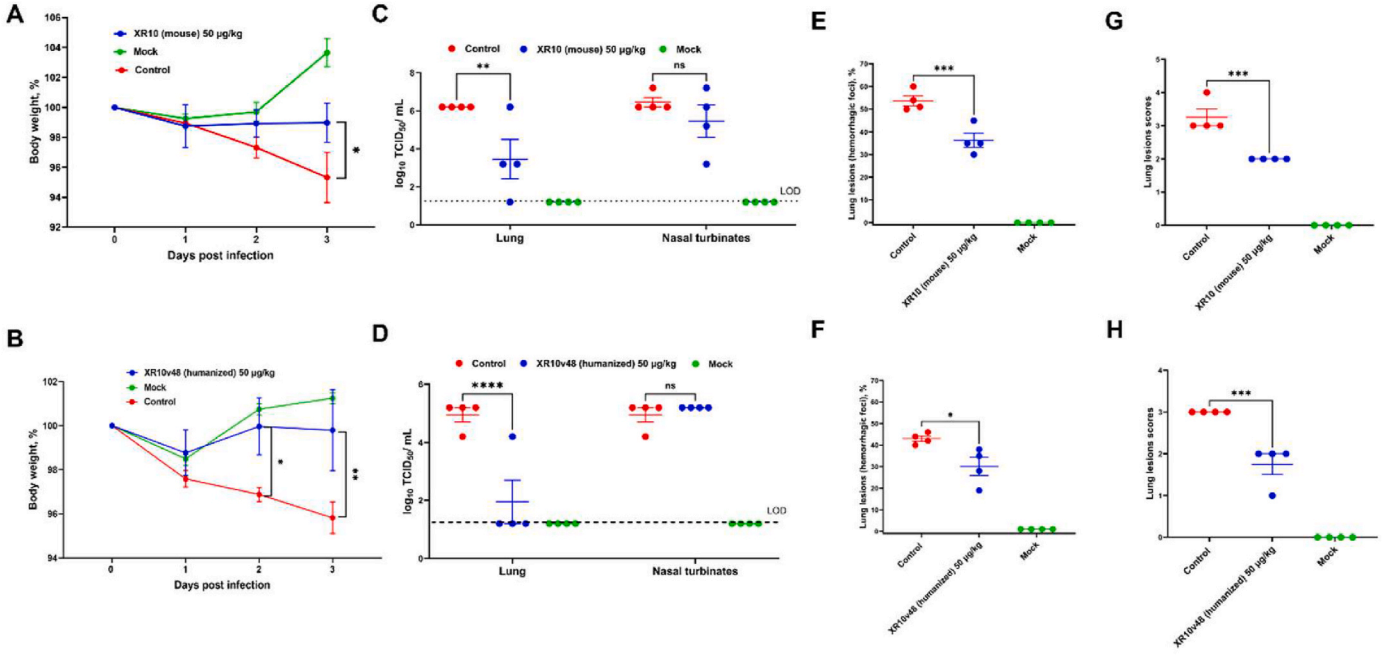

Fig. 4. Intranasal prophylactic SARS-CoV-2 protection of mouse and humanized XR10 mAb in Syrian hamsters. Shown are changes in body weight at 0–3 days after challenge and treatment with mouse XR10 **(A)** or XR10v48 **(B)**; viral load in nasal turbinates and lungs expressed as $\log_{10}$ $TCID_{50}$/mL on day 3 after challenge for mouse XR10 treatment **(C)** or XR10v48 administration **(D)**; lung lesions (hemorrhagic foci) **(E,F)** and lung histology analysis **(G,H)** on day 3 after challenge for mouse XR10 **(E,G)** or XR10v48 **(F,H)** administration. Differences between groups were assessed by Dunnett's multiple comparison test. $P < 0.05$ was considered significant. *$P < 0.05$, **$P < 0.01$ and ***$P < 0.001$ and ****$P < 0.0001$.

suggest that XR10v48 can be used in SARS-CoV-2 infection prophylaxis at a relatively low single-administration dose. In conclusion, CRVZ humanization yielded an antibody variant with >80 % homology to HGL, retained binding activity to SARS-CoV-2 spike, and *in vivo* protective activity.

4. Discussion

Recombinant monoclonal antibodies (mAb) represent promising candidates for therapy and prophylaxis of infectious diseases, as they are relatively stable and can be produced with high scalability. Moreover, intranasal delivery of mAb has been shown to confer viral protection in a prophylactic setting in humans and mice (Lin et al., 2022; Lu et al., 2022; Yang, 2021) and a therapeutic setting in hamsters (Haga et al., 2021). Various approaches can be used to generate human therapeutic mAb, including direct discovery from convalescent or vaccinated individuals or humanization of murine antibodies generated using hybridoma technology. In this study, we used hybridoma technology to generate a panel of neutralizing antibodies with high affinity towards the SARS-CoV-2 Spike protein. These mAbs bound to various spike epitopes overlapping with the ACE2 interaction zone and demonstrated strong binding with affinity up to 1.089 nM.

To decrease the probability of HAMA responses, we performed humanization of the generated antibodies. We used CRVZ humanization, a straightforward experiment-driven pipeline that allowed us to arrive at a high level of HGL homology (88.3 % and 87.2 % for XR10v43 and XR51v127) with nominal or higher affinity in comparison to the original murine mAb. While conventional CDR grafting approach can reach acceptable results in a short period of time, (Padlan, 1991), it does not account for non-CDR residues that can influence antigen binding. CRVZ explicitly considers the contribution of such residues thereby improving the likelihood of preserving antigen affinity. Antibody resurfacing, in contrast, retains the murine antibody backbone and introduces minimal changes limited to solvent-accessible residues in order to reduce immunogenicity. While this approach generally preserves binding affinity, it does not address the presence of potential T cell epitopes within the murine sequence, which may still elicit anti-drug immune responses. By using a fully human framework as a template, CRVZ helps to mitigate such risk. A key limitation of the CRVZ method is its reliance on iterative experimental testing, making the procedure more time-consuming than conventional CDR grafting or resurfacing strategies. In future, this can be addressed through automation and downscaling the antibody variant production and screening.

CRVZ can be further improved if combined with *in silico* humanization methods. For instance, recent advances in deep learning and language modeling combined with vast antibody repertoire databases yielded a platform able to humanize and evaluate the humanness of mouse mAbs, that suggested a similar set of amino acid exchanges for most of the sequences used in our study (Marks et al., 2021; Prihoda et al., 2022). Additionally, molecular dynamics simulations can be used to predict the effect of humanization on the mouse mAb function (Hsieh et al., 2022). It is important to highlight that these methods rely on a massive amount of experimental data that can be generated with an approach developed in this study. In future, we plan to implement a machine learning model to aid the humanization process and decrease the number of variants that have to be tested to select the optimal combination of humanization extent and neutralization.

Furthermore, humanization procedure might be circumvented by using genetically engineered mice (Laffleur et al., 2012) or phage display (Marks et al., 1991), however, these techniques might be technically complex and of limited availability.

It is important to note that, despite the widespread use of humanization procedure, the immunogenicity of some therapeutic mAbs remains unpredictable. Even fully human mAbs have been shown to be immunogenic in clinical settings (Harding et al., 2010). Such responses might be triggered by various factors, including residual non-human sequences, post-translational modifications, or conformational elements that expose novel epitopes to the human immune system or lead to antibody aggregation (Vaisman-Mentesh et al., 2020). The risk might be exacerbated by the route of administration: mucosal delivery that was used in our study may enhance antigen uptake and presentation, potentially amplifying immune recognition (Kehagia et al., 2023). Several studies demonstrated favorable safety of intranasal mAb administration (Hu et al., 2024; Lin et al., 2022). In addition, methods such as removing T-cell epitopes (de-immunization (Parker et al., 2013)) or introducing T-reg epitopes (tolerization (Cousens et al., 2013; Groot et al., 2013)) may be applied to mitigate any anti-therapeutic response and can be combined with the CRVZ method.

The humanized XR10v48 (85.3 % homology to HGL) selected for *in vivo* testing was as efficient in protection as the original XR10 mouse variant. We showed protection against infection with SARS-CoV-2 Delta virus in Syrian hamster model at a single-dose nasal administration at a concentration of 50 μg/kg, which is substantially lower than previously reported nasal therapeutic antibodies (Haga et al., 2021). The delivery route chosen for XR10v48 offers a significant advantage for treatment and prophylaxis of respiratory viruses. Even though it is possible to prevent infection with high-dose intravenous mAb administration, systemic administration resulted in a poor distribution into the lung (Cruz-Teran et al., 2021; Respaud et al., 2015). Although we did not analyze the biodistribution of the mAb in the hamsters, we show the significant reduction of the viral load in the lung tissues, which suggests its successful delivery to the primary site of infection. Intranasal administration of IgG was previously shown to lead to FcRn-mediated uptake through the mucosa (Ladel et al., 2018). This can enhance processing by antigen-presenting cells (Halwe et al., 2021; Yoshida et al., 2004). These findings highlight the potential utility of intranasally delivered mAbs for SARS-CoV-2 prophylaxis.

In contrast to neutralizing antibodies derived from convalescent or vaccinated individuals, which often require additional affinity maturation or framework optimization to improve expression, stability, and manufacturability, our CRVZ strategy enables direct humanization of well-characterized murine mAbs. This approach empirically preserves antigen-binding affinity through Vernier zone optimization while achieving high human germline homology. The ability to rationally design and screen optimized variants makes CRVZ highly adaptable for rapid response against emerging pathogens, particularly when conserved or cryptic epitopes are difficult to access through natural immune responses. As such, this strategy provides a complementary path to conventional antibody discovery pipelines.

This study has notable limitations. One limitation is the absence of RT-qPCR data to quantify viral RNA load in respiratory tissues. While infectious virus titers measured by $TCID_{50}$ remain the gold standard for assessing replication-competent virus, qPCR analysis would offer an orthogonal and sensitive measure of viral burden, independent of potential *ex vivo* neutralization effects that may occur during tissue homogenization. In future studies, we aim to incorporate quantitative RT-PCR (targeting RdRp or subgenomic E genes) to complement virological and histopathological analyses, thereby providing a more comprehensive evaluation of antiviral efficacy.

Furthermore, we do not currently know how other approved mAbs against SARS-CoV-2 which are normally administered parenterally would perform if administered intranasally. Such a comparison would provide valuable experimental data that can instruct the administration route selection.

While studies using traditional crystallography or cryo-EM to solve the structures of XR10v48 bound to spike of Omicron SARS-CoV-2 and other variants were outside the scope of this study, such information would be highly beneficial to understand how XR10v48 displays activity against Delta, Wuhan and Omicron BA.1 variants, whereas other mAbs are much more restricted in their recognition of different spike variants. Given the rapidly evolving landscape of SARS-CoV-2 variants, further studies will be needed to expand XR10v48 neutralization data to include

XBB.1.5, JN.1 and other newer subvariants. The Syrian hamster model, while valuable for respiratory virus pathogenesis and therapeutic studies, is unlikely to fully recapitulate human mucosal immunology, including FcRn-mediated recycling and anatomical features of the upper respiratory tract. To enhance human translational relevance, follow-up studies will be needed in non-human primates (NHPs) and humanized FcRn transgenic mice to evaluate nasal mAb retention, systemic spillover, therapeutic dosing, pharmacokinetics (e.g., mAb half-life in nasal/lung tissues) and other features more reflective of human physiology.

In conclusion, the study presents a straightforward mAb humanization pipeline that does not require specialist structural knowledge and enabled the development of highly humanized antibodies with retained or improved functional SARS-CoV-2 viral activity. XR10v48 bound SARS-CoV-2 spike with subnanomolar affinity and when intranasally delivered provided a non-invasive alternative to injected therapeutic antibodies. Beyond SARS-CoV-2, the CRVZ pipeline and intranasal mAb delivery may be broadly applicable to other airborne pathogens such as influenza and RSV. Hence these data represents a proof of concept for an adaptable and scalable therapeutic antiviral mAb development platform.

CRediT authorship contribution statement

Mikhail Lebedin: Writing – original draft, Visualization, Validation, Resources, Project administration, Methodology, Investigation, Formal analysis, Data curation, Conceptualization. **Nikolai Petrovsky:** Writing – review & editing, Resources, Investigation, Funding acquisition, Formal analysis. **Kairat Tabynov:** Writing – review & editing, Visualization, Resources, Methodology, Investigation, Funding acquisition, Formal analysis, Data curation, Conceptualization. **Kaissar Tabynov:** Writing – review & editing, Visualization, Supervision, Resources, Methodology, Investigation, Funding acquisition, Formal analysis, Data curation, Conceptualization. **Yuri Lebedin:** Writing – review & editing, Visualization, Validation, Supervision, Resources, Project administration, Methodology, Investigation, Funding acquisition, Formal analysis, Data curation, Conceptualization.

ICMJE criteria statement

All authors attest they meet the ICMJE criteria for authorship.

Declaration of competing interest

The authors declare the following financial interests/personal relationships which may be considered as potential competing interests: Yuri Lebedin reports a relationship with Xema LLC that includes: employment. If there are other authors, they declare that they have no known competing financial interests or personal relationships that could have appeared to influence the work reported in this paper.

Acknowledgements

N.P. was supported by the funding from National Institute of Allergy and Infectious Diseases of the National Institutes of Health under Contracts HHS-N272201400053C and HHS-N272200800039C. The content is solely the responsibility of the authors and does not necessarily represent the official views of the National Institutes of Health. We would like to thank Dr. Mariia Sergeeva from Smorodintsev Research Institute of Influenza for performing pseudovirus neutralization assay. We extend our gratitude to Turebekov N. and Fomin G. for their diligent efforts in ensuring the biosecurity and safety aspects of our research, as well as for conducting the histological studies on hamster lung tissue samples. We also thank Zhambyrbayeva L.S. and Sarmantayeva K.B. for their exceptional care and maintenance of the hamsters.

Appendix A. Supplementary data

Supplementary data to this article can be found online at https://doi.org/10.1016/j.antiviral.2025.106235.

Data availability

All data are provided as supplementary Tables S1 and S2.

References

Aboud-Pirak, E., Hurwitz, E., Pirak, M.E., Bellot, F., Schlessinger, J., Sela, M., 1988. Efficacy of antibodies to epidermal growth factor receptor against KB carcinoma in vitro and in nude mice. Jnci. J. Nation. Cancer Inst. 80, 1605–1611. https://doi.org/10.1093/jnci/80.20.1605.

Amanat, F., Stadlbauer, D., Strohmeier, S., Nguyen, T.H.O., Chromikova, V., McMahon, M., Jiang, K., Arunkumar, G.A., Jurczyszak, D., Polanco, J., Bermudez-Gonzalez, M., Kleiner, G., Aydillo, T., Miorin, L., Fierer, D.S., Lugo, L.A., Kojic, E.M., Stoever, J., Liu, S.T.H., Cunningham-Rundles, C., Felgner, P.L., Moran, T., García-Sastre, A., Caplivski, D., Cheng, A.C., Kedzierska, K., Vapalahti, O., Hepojoki, J.M., Simon, V., Krammer, F., 2020. A serological assay to detect SARS-CoV-2 seroconversion in humans. Nat. Med. 26, 1033–1036. https://doi.org/10.1038/s41591-020-0913-5.

Barnes, C.O., Jette, C.A., Abernathy, M.E., Dam, K.-M.A., Esswein, S.R., Gristick, H.B., Malyutin, A.G., Sharaf, N.G., Huey-Tubman, K.E., Lee, Y.E., Robbiani, D.F., Nussenzweig, M.C., West, A.P., Bjorkman, P.J., 2020. SARS-CoV-2 neutralizing antibody structures inform therapeutic strategies. Nature 588, 682–687. https://doi.org/10.1038/s41586-020-2852-1.

Butt, A.A., Dargham, S.R., Chemaitelly, H., Khal, A.A., Tang, P., Hasan, M.R., Coyle, P.V., Thomas, A.G., Borham, A.M., Concepcion, E.G., Kaleeckal, A.H., Latif, A.N., Bertollini, R., Abou-Samra, A.-B., Abu-Raddad, L.J., 2022. Severity of illness in persons infected with the SARS-CoV-2 delta variant vs beta variant in Qatar. JAMA Intern. Med. 182, 197–205. https://doi.org/10.1001/jamainternmed.2021.7949.

Cao, C., Cai, Z., Xiao, X., Rao, J., Chen, J., Hu, N., Yang, M., Xing, X., Wang, Y., Li, M., Zhou, B., Wang, X., Wang, J., Xue, Y., 2021. The architecture of the SARS-CoV-2 RNA genome inside virion. Nat. Commun. 12, 3917. https://doi.org/10.1038/s41467-021-22785-x.

Chen, Y., Zhao, X., Zhou, H., Zhu, H., Jiang, S., Wang, P., 2023. Broadly neutralizing antibodies to SARS-CoV-2 and other human coronaviruses. Nat. Rev. Immunol. 23, 189–199. https://doi.org/10.1038/s41577-022-00784-3.

Chi, X., Yan, R., Zhang, Jun, Zhang, G., Zhang, Y., Hao, M., Zhang, Z., Fan, P., Dong, Y., Yang, Y., Chen, Z., Guo, Y., Zhang, Jinlong, Li, Y., Song, X., Chen, Y., Xia, L., Fu, L., Hou, L., Xu, J., Yu, C., Li, J., Zhou, Q., Chen, W., 2020. A neutralizing human antibody binds to the N-terminal domain of the Spike protein of SARS-CoV-2. Science 369, 650–655. https://doi.org/10.1126/science.abc6952.

Cousens, L., Moise, L., Terry, F., Martin, W., Groot, A.D., 2013. Immunogenic biologics: validation of screening, deimmunization and tolerization approaches (P3251). J. Immunol. 190. https://doi.org/10.4049/jimmunol.190.supp.192.11, 192.11-192.11.

Cruz-Teran, C., Tiruthani, K., McSweeney, M., Ma, A., Pickles, R., Lai, S.K., 2021. Challenges and opportunities for antiviral monoclonal antibodies as COVID-19 therapy. Adv. Drug Deliv. Rev. 169, 100–117. https://doi.org/10.1016/j.addr.2020.12.004.

Dejnirattisai, W., Zhou, D., Ginn, H.M., Duyvesteyn, H.M.E., Supasa, P., Case, J.B., Zhao, Y., Walter, T.S., Mentzer, A.J., Liu, C., Wang, B., Paesen, G.C., Slon-Campos, J., López-Camacho, C., Kafai, N.M., Bailey, A.L., Chen, R.E., Ying, B., Thompson, C., Bolton, J., Fyfe, A., Gupta, S., Tan, T.K., Gilbert-Jaramillo, J., James, W., Knight, M., Carroll, M.W., Skelly, D., Dold, C., Peng, Y., Levin, R., Dong, T., Pollard, A.J., Knight, J.C., Klenerman, P., Temperton, N., Hall, D.R., Williams, M.A., Paterson, N.G., Bertram, F.K.R., Siebert, C.A., Clare, D.K., Howe, A., Radecke, J., Song, Y., Townsend, A.R., Huang, K.-Y.A., Fry, E.E., Mongkolsapaya, J., Diamond, M.S., Ren, J., Stuart, D.I., Screaton, G.R., 2021. The antigenic anatomy of SARS-CoV-2 receptor binding domain. Cell 184, 2183–2200.e22. https://doi.org/10.1016/j.cell.2021.02.032.

Dickey, T.H., Tang, W.K., Butler, B., Ouahes, T., Orr-Gonzalez, S., Salinas, N.D., Lambert, L.E., Tolia, N.H., 2022. Design of the SARS-CoV-2 RBD vaccine antigen improves neutralizing antibody response. Sci. Adv. 8, eabq8276. https://doi.org/10.1126/sciadv.abq8276.

Fan, Y., Li, X., Zhang, Lei, Wan, S., Zhang, Long, Zhou, F., 2022. SARS-CoV-2 Omicron variant: recent progress and future perspectives. Signal Transduct. Targeted Ther. 7, 141. https://doi.org/10.1038/s41392-022-00997-x.

Ferrara, N., Hillan, K.J., Gerber, H.-P., Novotny, W., 2004. Discovery and development of bevacizumab, an anti-VEGF antibody for treating cancer. Nat. Rev. Drug Discov. 3, 391–400. https://doi.org/10.1038/nrd1381.

Foote, J., Winter, G., 1992. Antibody framework residues affecting the conformation of the hypervariable loops. J. Mol. Biol. 224, 487–499. https://doi.org/10.1016/0022-2836(92)91010-m.

Frenzel, A., Schirrmann, T., Hust, M., 2016. Phage display-derived human antibodies in clinical development and therapy. mAbs 8, 1177–1194. https://doi.org/10.1080/19420862.2016.1212149.

Ge, J., Wang, R., Ju, B., Zhang, Q., Sun, J., Chen, P., Zhang, S., Tian, Y., Shan, S., Cheng, L., Zhou, B., Song, S., Zhao, Juanjuan, Wang, H., Shi, X., Ding, Q., Liu, L., Zhao, Jincun, Zhang, Z., Wang, X., Zhang, L., 2021. Antibody neutralization of SARS-

CoV-2 through ACE2 receptor mimicry. Nat. Commun. 12, 250. https://doi.org/10.1038/s41467-020-20501-9.
Groot, A.S.D., Terry, F., Cousens, L., Martin, W., 2013. Beyond humanization and de-immunization: tolerization as a method for reducing the immunogenicity of biologics. Expet Rev. Clin. Pharmacol. 6, 651–662. https://doi.org/10.1586/17512433.2013.835698.
Haga, K., Takai-Todaka, R., Matsumura, Y., Song, C., Takano, T., Tojo, T., Nagami, A., Ishida, Y., Masaki, H., Tsuchiya, M., Ebisudani, T., Sugimoto, S., Sato, T., Yasuda, H., Fukunaga, K., Sawada, A., Nemoto, N., Murata, K., Morimoto, T., Katayama, K., 2021. Nasal delivery of single-domain antibody improves symptoms of SARS-CoV-2 infection in an animal model. PLoS Pathog. 17, e1009542. https://doi.org/10.1371/journal.ppat.1009542.
Halwe, S., Kupke, A., Vanshylla, K., Liberta, F., Gruell, H., Zehner, M., Rohde, C., Krähling, V., Serra, M.G., Kreer, C., Klüver, M., Sauerhering, L., Schmidt, J., Cai, Z., Han, F., Young, D., Yang, G., Widera, M., Koch, M., Werner, A., Kämper, L., Becker, N., Marlow, M.S., Eickmann, M., Ciesek, S., Schiele, F., Klein, F., Becker, S., 2021. Intranasal administration of a monoclonal neutralizing antibody protects mice against SARS-CoV-2 infection. Viruses 13, 1498. https://doi.org/10.3390/v13081498.
Hansen, J., Baum, A., Pascal, K.E., Russo, V., Giordano, S., Wloga, E., Fulton, B.O., Yan, Y., Koon, K., Patel, K., Chung, K.M., Hermann, A., Ullman, E., Cruz, J., Rafique, A., Huang, T., Fairhurst, J., Libertiny, C., Malbec, M., Lee, W., Welsh, R., Farr, G., Pennington, S., Deshpande, D., Cheng, J., Watty, A., Bouffard, P., Babb, R., Levenkova, N., Chen, C., Zhang, B., Hernandez, A.R., Saotome, K., Zhou, Y., Franklin, M., Sivapalasingam, S., Lye, D.C., Weston, S., Logue, J., Haupt, R., Frieman, M., Chen, G., Olson, W., Murphy, A.J., Stahl, N., Yancopoulos, G.D., Kyratsous, C.A., 2020. Studies in humanized mice and convalescent humans yield a SARS-CoV-2 antibody cocktail. Science 369, 1010–1014. https://doi.org/10.1126/science.abd0827.
Harding, F.A., Stickler, M.M., Razo, J., DuBridge, R., 2010. The immunogenicity of humanized and fully human antibodies. mAbs 2, 256–265. https://doi.org/10.4161/mabs.2.3.11641.
Hoffmann, M., Krüger, N., Schulz, S., Cossmann, A., Rocha, C., Kempf, A., Nehlmeier, I., Graichen, L., Moldenhauer, A.-S., Winkler, M.S., Lier, M., Dopfer-Jablonka, A., Jäck, H.-M., Behrens, G.M.N., Pöhlmann, S., 2022. The Omicron variant is highly resistant against antibody-mediated neutralization: implications for control of the COVID-19 pandemic. Cell 185, 447–456.e11. https://doi.org/10.1016/j.cell.2021.12.032.
Hsieh, Y.-C., Liao, J., Chuang, K.-H., Ho, K.-W., Hong, S.-T., Liu, H.-J., Huang, B.-C., Chen, I.-J., Liu, Y.-L., Wang, J.-Y., Tsai, H.-L., Su, Y.-C., Wang, Y.-T., Cheng, T.-L., 2022. A universal in silico V(D)J recombination strategy for developing humanized monoclonal antibodies. J. Nanobiotechnol. 20, 58. https://doi.org/10.1186/s12951-022-01259-2.
Hu, C., Zhou, Y., Meng, X., Li, J., Chen, J., Ying, Z., Xie, X.S., Hu, Y., Cao, Y., Jin, R., 2024. Safety and intranasal retention of a broad-spectrum anti-SARS-CoV-2 monoclonal antibody SA55 nasal spray in healthy volunteers: a phase I clinical trial. Pharmaceutics 17, 43. https://doi.org/10.3390/pharmaceutics17010043.
Huang, C., Wang, Y., Li, X., Ren, L., Zhao, J., Hu, Y., Zhang, L., Fan, G., Xu, J., Gu, X., Cheng, Z., Yu, T., Xia, J., Wei, Y., Wu, W., Xie, X., Yin, W., Li, H., Liu, M., Xiao, Y., Gao, H., Guo, L., Xie, J., Wang, G., Jiang, R., Gao, Z., Jin, Q., Wang, J., Cao, B., 2020. Clinical features of patients infected with 2019 novel coronavirus in Wuhan, China. Lancet 395, 497–506. https://doi.org/10.1016/s0140-6736(20)30183-5.
Investigators, T.E., 1994. Use of a monoclonal antibody directed against the platelet glycoprotein IIb/IIIa receptor in high-risk coronary angioplasty. N. Engl. J. Med. 330, 956–961. https://doi.org/10.1056/nejm199404073301402.
Jacobson, J.M., Kuritzkes, D.R., Godofsky, E., DeJesus, E., Larson, J.A., Weinheimer, S.P., Lewis, S.T., 2009. Safety, pharmacokinetics, and antiretroviral activity of multiple doses of ibalizumab (formerly TNX-355), an anti-CD4 monoclonal antibody, in human immunodeficiency virus type 1-infected adults. Antimicrob. Agents Chemother. 53, 450–457. https://doi.org/10.1128/aac.00942-08.
Jia, Y., Niu, S., Hu, Y., Chai, Y., Zheng, A., Su, C., Wu, L., Han, Pengcheng, Han, Pu, Lu, D., Liu, Z., Yan, X., Tian, D., Chen, Z., Qi, J., Tian, W., Wang, Q., Gao, G.F., 2022. Cross-reaction of current available SARS-CoV-2 MAbs against the pangolin-origin coronavirus GX/P2V/2017. Cell Rep. 41, 111831. https://doi.org/10.1016/j.celrep.2022.111831.
Ju, B., Zhang, Q., Ge, J., Wang, R., Sun, J., Ge, X., Yu, Jiazhen, Shan, S., Zhou, B., Song, S., Tang, X., Yu, Jinfang, Lan, J., Yuan, J., Wang, H., Zhao, Juanjuan, Zhang, S., Wang, Y., Shi, X., Liu, L., Zhao, Jincun, Wang, X., Zhang, Z., Zhang, L., 2020. Human neutralizing antibodies elicited by SARS-CoV-2 infection. Nature 584, 115–119. https://doi.org/10.1038/s41586-020-2380-z.
Jumper, J., Evans, R., Pritzel, A., Green, T., Figurnov, M., Ronneberger, O., Tunyasuvunakool, K., Bates, R., Žídek, A., Potapenko, A., Bridgland, A., Meyer, C., Kohl, S.A.A., Ballard, A.J., Cowie, A., Romera-Paredes, B., Nikolov, S., Jain, R., Adler, J., Back, T., Petersen, S., Reiman, D., Clancy, E., Zielinski, M., Steinegger, M., Pacholska, M., Berghammer, T., Bodenstein, S., Silver, D., Vinyals, O., Senior, A.W., Kavukcuoglu, K., Kohli, P., Hassabis, D., 2021. Highly accurate protein structure prediction with AlphaFold. Nature 596, 583–589. https://doi.org/10.1038/s41586-021-03819-2.
Kehagia, E., Papakyriakopoulou, P., Valsami, G., 2023. Advances in intranasal vaccine delivery: a promising non-invasive route of immunization. Vaccine 41, 3589–3603. https://doi.org/10.1016/j.vaccine.2023.05.011.
Kempeni, J., 1999. Preliminary results of early clinical trials with the fully human anti-TNFα monoclonal antibody D2E7. Ann. Rheum. Dis. 58, I70. https://doi.org/10.1136/ard.58.2008.i70.
Köhler, G., Milstein, C., 1975. Continuous cultures of fused cells secreting antibody of predefined specificity. Nature 256, 495–497. https://doi.org/10.1038/256495a0.
Ladel, S., Flamm, J., Zadeh, A.S., Filzwieser, D., Walter, J.-C., Schlossbauer, P., Kinscherf, R., Lischka, K., Luksch, H., Schindowski, K., 2018. Allogenic Fc domain-facilitated uptake of IgG in nasal lamina propria: friend or foe for intranasal CNS delivery? Pharmaceutics 10, 107. https://doi.org/10.3390/pharmaceutics10030107.
Laffleur, B., Pascal, V., Sirac, C., Cogné, M., 2012. Antibody methods and protocols. Methods Mol. Biol. 901, 149–159. https://doi.org/10.1007/978-1-61779-931-0_9.
Lan, J., Ge, J., Yu, J., Shan, S., Zhou, H., Fan, S., Zhang, Q., Shi, X., Wang, Q., Zhang, L., Wang, X., 2020. Structure of the SARS-CoV-2 spike receptor-binding domain bound to the ACE2 receptor. Nature 581, 215–220. https://doi.org/10.1038/s41586-020-2180-5.
Lin, Y., Yue, S., Yang, Y., Yang, S., Pan, Z., Yang, X., Gao, L., Zhou, J., Li, Z., Hu, L., Tang, J., Wu, Q., Lei, S., Tian, Q., Wang, Y., Hao, Y., Xu, L., Huang, Q., Zhu, B., Chen, Y., Chen, X., Ye, L., 2022. Nasal spray of neutralizing monoclonal antibody 35B5 confers potential prophylaxis against severe acute respiratory syndrome coronavirus 2 variants of concern: a small-scale clinical trial. Clin. Infect. Dis. 76, e336–e341. https://doi.org/10.1093/cid/ciac448.
Liu, Lihong, Iketani, S., Guo, Y., Chan, J.F.-W., Wang, M., Liu, Liyuan, Luo, Y., Chu, H., Huang, Yiming, Nair, M.S., Yu, J., Chik, K.K.-H., Yuen, T.T.-T., Yoon, C., To, K.K.-W., Chen, H., Yin, M.T., Sobieszczyk, M.E., Huang, Yaoxing, Wang, H.H., Sheng, Z., Yuen, K.-Y., Ho, D.D., 2022. Striking antibody evasion manifested by the Omicron variant of SARS-CoV-2. Nature 602, 676–681. https://doi.org/10.1038/s41586-021-04388-0.
Lonberg, N., Taylor, L.D., Harding, F.A., Trounstine, M., Higgins, K.M., Schramm, S.R., Kuo, C.-C., Mashayekh, R., Wymore, K., McCabe, J.G., Munoz-O'Regan, D., O'Donnell, S.L., Lapachet, E.S.G., Bengoechea, T., Fishwild, D.M., Carmack, C.E., Kay, R.M., Huszar, D., 1994. Antigen-specific human antibodies from mice comprising four distinct genetic modifications. Nature 368, 856–859. https://doi.org/10.1038/368856a0.
Lu, J., Yin, Q., Pei, R., Zhang, Q., Qu, Y., Pan, Y., Sun, L., Gao, D., Liang, C., Yang, J., Wu, W., Li, J., Cui, Z., Wang, Z., Li, X., Li, D., Wang, S., Duan, K., Guan, W., Liang, M., Yang, X., 2022. Nasal delivery of broadly neutralizing antibodies protects mice from lethal challenge with SARS-CoV-2 delta and omicron variants. Virol. Sin. 37, 238–247. https://doi.org/10.1016/j.virs.2022.02.005.
Lu, R.-M., Hwang, Y.-C., Liu, I.-J., Lee, C.-C., Tsai, H.-Z., Li, H.-J., Wu, H.-C., 2020. Development of therapeutic antibodies for the treatment of diseases. J. Biomed. Sci. 27, 1. https://doi.org/10.1186/s12929-019-0592-z.
Lu, R.-M., Liang, K.-H., Chiang, H.-L., Hsu, F.-F., Lin, H.-T., Chen, W.-Y., Ke, F.-Y., Kumari, M., Chou, Y.-C., Tao, M.-H., Lin, Y.-L., Wu, H.-C., 2023. Broadly neutralizing antibodies against Omicron variants of SARS-CoV-2 derived from mRNA-lipid nanoparticle-immunized mice. Heliyon 9, e15587. https://doi.org/10.1016/j.heliyon.2023.e15587.
Makabe, K., Nakanishi, T., Tsumoto, K., Tanaka, Y., Kondo, H., Umetsu, M., Sone, Y., Asano, R., Kumagai, I., 2008. Thermodynamic consequences of mutations in vernier zone residues of a humanized anti-human epidermal growth factor receptor murine antibody, 528. J. Biol. Chem. 283, 1156–1166. https://doi.org/10.1074/jbc.m706190200.
Maloney, D.G., Grillo-López, A.J., White, C.A., Bodkin, D., Schilder, R.J., Neidhart, J.A., Janakiraman, N., Foon, K.A., Liles, T.-M., Dallaire, B.K., Wey, K., Royston, I., Davis, T., Levy, R., 1997. IDEC-C2B8 (Rituximab) anti-CD20 monoclonal antibody therapy in patients with relapsed low-grade non-Hodgkin's Lymphoma. Blood 90, 2188–2195. https://doi.org/10.1182/blood.v90.6.2188.
Marks, C., Hummer, A.M., Chin, M., Deane, C.M., 2021. Humanization of antibodies using a machine learning approach on large-scale repertoire data. Bioinformatics 37, 4041–4047. https://doi.org/10.1093/bioinformatics/btab434.
Marks, J.D., Hoogenboom, H.R., Bonnert, T.P., McCafferty, J., Griffiths, A.D., Winter, G., 1991. By-passing immunization Human antibodies from V-gene libraries displayed on phage. J. Mol. Biol. 222, 581–597. https://doi.org/10.1016/0022-2836(91)90498-u.
Olsson, P.G., Hammarström, L., Smith, C.I.E., 1991. Antigenicity of mouse monoclonal antibodies. A study on the variable region of the heavy chain. J. Theor. Biol. 151, 111–122. https://doi.org/10.1016/s0022-5193(05)80146-8.
Padlan, E.A., 1991. A possible procedure for reducing the immunogenicity of antibody variable domains while preserving their ligand-binding properties. Mol. Immunol. 28, 489–498. https://doi.org/10.1016/0161-5890(91)90163-e.
Parker, A.S., Choi, Y., Griswold, K.E., Bailey-Kellogg, C., 2013. Structure-guided deimmunization of therapeutic proteins. J. Comput. Biol. 20, 152–165. https://doi.org/10.1089/cmb.2012.0251.
Pascalis, R.D., Iwahashi, M., Tamura, M., Padlan, E.A., Gonzales, N.R., Santos, A.D., Giuliano, M., Schuck, P., Schlom, J., Kashmiri, S.V.S., 2002. Grafting of "Abbreviated" complementarity-determining regions containing specificity-determining residues essential for ligand contact to engineer a less immunogenic humanized monoclonal antibody. J. Immunol. 169, 3076–3084. https://doi.org/10.4049/jimmunol.169.6.3076.
Pavlinkova, G., Colcher, D., Booth, B.J.M., Goel, A., Wittel, U.A., Batra, S.K., 2001. Effects of humanization and gene shuffling on immunogenicity and antigen binding of anti-tag-72 single-chain Fvs. Int. J. Cancer 94, 717–726. https://doi.org/10.1002/ijc.1523.
Piccoli, L., Park, Y.-J., Tortorici, M.A., Czudnochowski, N., Walls, A.C., Beltramello, M., Silacci-Fregni, C., Pinto, D., Rosen, L.E., Bowen, J.E., Acton, O.J., Jaconi, S., Guarino, B., Minola, A., Zatta, F., Sprugasci, N., Bassi, J., Peter, A., Marco, A.D., Nix, J.C., Mele, F., Jovic, S., Rodriguez, B.F., Gupta, S.V., Jin, F., Piumatti, G., Presti, G.L., Pellanda, A.F., Biggiogero, M., Tarkowski, M., Pizzuto, M.S., Cameroni, E., Havenar-Daughton, C., Smithey, M., Hong, D., Lepori, V., Albanese, E., Ceschi, A., Bernasconi, E., Elzi, L., Ferrari, P., Garzoni, C., Riva, A., Snell, G., Sallusto, F., Fink, K., Virgin, H.W., Lanzavecchia, A., Corti, D., Veesler, D., 2020.

Mapping neutralizing and immunodominant sites on the SARS-CoV-2 spike receptor-binding domain by structure-guided high-resolution serology. Cell 183, 1024–1042. e21. https://doi.org/10.1016/j.cell.2020.09.037.

Pinto, D., Park, Y.-J., Beltramello, M., Walls, A.C., Tortorici, M.A., Bianchi, S., Jaconi, S., Culap, K., Zatta, F., Marco, A.D., Peter, A., Guarino, B., Spreafico, R., Cameroni, E., Case, J.B., Chen, R.E., Havenar-Daughton, C., Snell, G., Telenti, A., Virgin, H.W., Lanzavecchia, A., Diamond, M.S., Fink, K., Veesler, D., Corti, D., 2020. Cross-neutralization of SARS-CoV-2 by a human monoclonal SARS-CoV antibody. Nature 583, 290–295. https://doi.org/10.1038/s41586-020-2349-y.

Planas, D., Saunders, N., Maes, P., Guivel-Benhassine, F., Planchais, C., Buchrieser, J., Bolland, W.-H., Porrot, F., Staropoli, I., Lemoine, F., Péré, H., Veyer, D., Puech, J., Rodary, J., Baele, G., Dellicour, S., Raymenants, J., Gorissen, S., Geenen, C., Vanmechelen, B., Wawina-Bokalanga, T., Martí-Carreras, J., Cuypers, L., Sève, A., Hocqueloux, L., Prazuck, T., Rey, F.A., Simon-Loriere, E., Bruel, T., Mouquet, H., André, E., Schwartz, O., 2022. Considerable escape of SARS-CoV-2 Omicron to antibody neutralization. Nature 602, 671–675. https://doi.org/10.1038/s41586-021-04389-z.

Pollack, P., Groothuis, J.R., Barbarotto, G.M., 2002. Development and use of palivizumab (Synagis): a passive immunoprophylactic agent for RSV. J. Infect. Chemother. 8, 201–206. https://doi.org/10.1007/s10156-002-0178-6.

Prihoda, D., Maamary, J., Waight, A., Juan, V., Fayadat-Dilman, L., Svozil, D., Bitton, D. A., 2022. BioPhi: a platform for antibody design, humanization, and humanness evaluation based on natural antibody repertoires and deep learning. mAbs 14, 2020203. https://doi.org/10.1080/19420862.2021.2020203.

RCoreTeam, 2019. R: a language and environment for statistical computing [WWW Document]. URL. https://www.R-project.org/.

Respaud, R., Vecellio, L., Diot, P., Heuzé-Vourc'h, N., 2015. Nebulization as a delivery method for mAbs in respiratory diseases. Expet Opin. Drug Deliv. 12, 1027–1039. https://doi.org/10.1517/17425247.2015.999039.

Robbiani, D.F., Gaebler, C., Muecksch, F., Lorenzi, J.C.C., Wang, Z., Cho, A., Agudelo, M., Barnes, C.O., Gazumyan, A., Finkin, S., Hägglöf, T., Oliveira, T.Y., Viant, C., Hurley, A., Hoffmann, H.-H., Millard, K.G., Kost, R.G., Cipolla, M., Gordon, K., Bianchini, F., Chen, S.T., Ramos, V., Patel, R., Dizon, J., Shimeliovich, I., Mendoza, P., Hartweger, H., Nogueira, L., Pack, M., Horowitz, J., Schmidt, F., Weisblum, Y., Michailidis, E., Ashbrook, A.W., Waltari, E., Pak, J.E., Huey-Tubman, K.E., Koranda, N., Hoffman, P.R., West, A.P., Rice, C.M., Hatziioannou, T., Bjorkman, P.J., Bieniasz, P.D., Caskey, M., Nussenzweig, M.C., 2020. Convergent antibody responses to SARS-CoV-2 in convalescent individuals. Nature 584, 437–442. https://doi.org/10.1038/s41586-020-2456-9.

Rogers, T.F., Zhao, F., Huang, D., Beutler, N., Burns, A., He, W., Limbo, O., Smith, C., Song, G., Woehl, J., Yang, L., Abbott, R.K., Callaghan, S., Garcia, E., Hurtado, J., Parren, M., Peng, L., Ramirez, S., Ricketts, J., Ricciardi, M.J., Rawlings, S.A., Wu, N. C., Yuan, M., Smith, D.M., Nemazee, D., Teijaro, J.R., Voss, J.E., Wilson, I.A., Andrabi, R., Briney, B., Landais, E., Sok, D., Jardine, J.G., Burton, D.R., 2020. Isolation of potent SARS-CoV-2 neutralizing antibodies and protection from disease in a small animal model. Science 369, 956–963. https://doi.org/10.1126/science.abc7520.

Saville, J.W., Mannar, D., Zhu, X., Berezuk, A.M., Cholak, S., Tuttle, K.S., Vahdatihassani, F., Subramaniam, S., 2023. Structural analysis of receptor engagement and antigenic drift within the BA.2 spike protein. Cell Rep. 42, 111964. https://doi.org/10.1016/j.celrep.2022.111964.

Shawler, D.L., Bartholomew, R.M., Smith, L.M., Dillman, R.O., 1985. Human immune response to multiple injections of murine monoclonal IgG. J. Immunol. 135, 1530–1535. https://doi.org/10.4049/jimmunol.135.2.1530.

Solomadin, M., Tabynov, Kairat, Petrovsky, N., Tabynov, Kaissar, 2023. Evaluation of a SARS-CoV-2 spike protein ectodomain subunit vaccine with a squalene emulsion adjuvant in rodents and rhesus macaques. Hum. Vaccines Immunother. 19, 2258571. https://doi.org/10.1080/21645515.2023.2258571.

Todd, P.A., Brogden, R.N., 1989. Muromonab CD3. Drugs 37, 871–899. https://doi.org/10.2165/00003495-198937060-00004.

Vaisman-Mentesh, A., Gutierrez-Gonzalez, M., DeKosky, B.J., Wine, Y., 2020. The molecular mechanisms that underlie the immune biology of anti-drug antibody formation following treatment with monoclonal antibodies. Front. Immunol. 11. https://doi.org/10.3389/fimmu.2020.01951, 1951.

Walls, A.C., Park, Y.-J., Tortorici, M.A., Wall, A., McGuire, A.T., Veesler, D., 2020. Structure, function, and antigenicity of the SARS-CoV-2 spike glycoprotein. Cell 181, 281–292.e6. https://doi.org/10.1016/j.cell.2020.02.058.

Wang, P., Nair, M.S., Liu, L., Iketani, S., Luo, Y., Guo, Y., Wang, M., Yu, J., Zhang, B., Kwong, P.D., Graham, B.S., Mascola, J.R., Chang, J.Y., Yin, M.T., Sobieszczyk, M., Kyratsous, C.A., Shapiro, L., Sheng, Z., Huang, Y., Ho, D.D., 2021. Antibody resistance of SARS-CoV-2 variants B.1.351 and B.1.1.7. Nature 593, 130–135. https://doi.org/10.1038/s41586-021-03398-2.

Wang, X., Zhang, L., Ge, J., 2022. Crystal structure of SARS-CoV-2 RBD with P2C-1F11 and P2B-1G5. https://doi.org/10.2210/pdb8gx9/pdb.

Westendorf, K., Žentelis, S., Wang, L., Foster, D., Vaillancourt, P., Wiggin, M., Lovett, E., Lee, R. van der, Hendle, J., Pustilnik, A., Sauder, J.M., Kraft, L., Hwang, Y., Siegel, R. W., Chen, J., Heinz, B.A., Higgs, R.E., Kallewaard, N.L., Jepson, K., Goya, R., Smith, M.A., Collins, D.W., Pellacani, D., Xiang, P., Puyraimond, V. de, Ricicova, M., Devorkin, L., Pritchard, C., O'Neill, A., Dalal, K., Panwar, P., Dhupar, H., Garces, F. A., Cohen, C.A., Dye, J.M., Huie, K.E., Badger, C.V., Kobasa, D., Audet, J., Freitas, J. J., Hassanali, S., Hughes, I., Munoz, L., Palma, H.C., Ramamurthy, B., Cross, R.W., Geisbert, T.W., Menachery, V., Lokugamage, K., Borisevich, V., Lanz, I., Anderson, L., Sipahimalani, P., Corbett, K.S., Yang, E.S., Zhang, Y., Shi, W., Zhou, T., Choe, M., Misasi, J., Kwong, P.D., Sullivan, N.J., Graham, B.S., Fernandez, T.L., Hansen, C.L., Falconer, E., Mascola, J.R., Jones, B.E., Barnhart, B.C., 2022. LY-CoV1404 (bebtelovimab) potently neutralizes SARS-CoV-2 variants. Cell Rep. 39, 110812. https://doi.org/10.1016/j.celrep.2022.110812.

Wu, X., Yang, Z.-Y., Li, Y., Hogerkorp, C.-M., Schief, W.R., Seaman, M.S., Zhou, T., Schmidt, S.D., Wu, L., Xu, L., Longo, N.S., McKee, K., O'Dell, S., Louder, M.K., Wycuff, D.L., Feng, Y., Nason, M., Doria-Rose, N., Connors, M., Kwong, P.D., Roederer, M., Wyatt, R.T., Nabel, G.J., Mascola, J.R., 2010. Rational design of envelope identifies broadly neutralizing human monoclonal antibodies to HIV-1. Science 329, 856–861. https://doi.org/10.1126/science.1187659.

Yang, L.Y.L., 2021. Nasal Delivery of Thermostable and Broadly Neutralizing Antibodies Protects Mice against SARS-CoV-2 Infection. Science Data Bank. https://doi.org/10.11922/sciencedb.01269.

Yoshida, M., Claypool, S.M., Wagner, J.S., Mizoguchi, E., Mizoguchi, A., Roopenian, D. C., Lencer, W.I., Blumberg, R.S., 2004. Human neonatal Fc receptor mediates transport of IgG into luminal secretions for delivery of antigens to mucosal dendritic cells. Immunity 20, 769–783. https://doi.org/10.1016/j.immuni.2004.05.007.

Yuan, M., Liu, H., Wu, N.C., Lee, C.-C.D., Zhu, X., Zhao, F., Huang, D., Yu, W., Hua, Y., Tien, H., Rogers, T.F., Landais, E., Sok, D., Jardine, J.G., Burton, D.R., Wilson, I.A., 2020. Structural basis of a shared antibody response to SARS-CoV-2. Science 369, 1119–1123. https://doi.org/10.1126/science.abd2321.

Zhou, D., Duyvesteyn, H.M.E., Chen, C.-P., Huang, C.-G., Chen, T.-H., Shih, S.-R., Lin, Y.-C., Cheng, C.-Y., Cheng, S.-H., Huang, Y.-C., Lin, T.-Y., Ma, C., Huo, J., Carrique, L., Malinauskas, T., Ruza, R.R., Shah, P.N.M., Tan, T.K., Rijal, P., Donat, R.F., Godwin, K., Buttigieg, K.R., Tree, J.A., Radecke, J., Paterson, N.G., Supasa, P., Mongkolsapaya, J., Screaton, G.R., Carroll, M.W., Gilbert-Jaramillo, J., Knight, M.L., James, W., Owens, R.J., Naismith, J.H., Townsend, A.R., Fry, E.E., Zhao, Y., Ren, J., Stuart, D.I., Huang, K.-Y.A., 2020. Structural basis for the neutralization of SARS-CoV-2 by an antibody from a convalescent patient. Nat. Struct. Mol. Biol. 27, 950–958. https://doi.org/10.1038/s41594-020-0480-y.